

International Journal of Engine Research

<http://jer.sagepub.com/>

Thermodynamic sweet spot for high-efficiency, dilute, boosted gasoline engines
George Lavoie, Elliott Ortiz-Soto, Aristotelis Babajimopoulos, Jason B. Martz and Dennis N. Assanis
International Journal of Engine Research published online 16 August 2012
DOI: 10.1177/1468087412455372

The online version of this article can be found at:
<http://jer.sagepub.com/content/early/2012/08/16/1468087412455372>

Published by:



<http://www.sagepublications.com>

On behalf of:



[Institution of Mechanical Engineers](#)

Additional services and information for *International Journal of Engine Research* can be found at:

Email Alerts: <http://jer.sagepub.com/cgi/alerts>

Subscriptions: <http://jer.sagepub.com/subscriptions>

Reprints: <http://www.sagepub.com/journalsReprints.nav>

Permissions: <http://www.sagepub.com/journalsPermissions.nav>

>> [OnlineFirst Version of Record - Aug 16, 2012](#)

[What is This?](#)

Thermodynamic sweet spot for high-efficiency, dilute, boosted gasoline engines

International J of Engine Research

0(0) 1–19

© IMechE 2012

Reprints and permissions:

sagepub.co.uk/journalsPermissions.nav

DOI: 10.1177/1468087412455372

jers.sagepub.com



**George A Lavoie, Elliott Ortiz-Soto, Aristotelis Babajimopoulos,
Jason B Martz and Dennis N Assanis**

Abstract

Recent developments in ignition, boosting, and control systems have opened up new opportunities for highly dilute, high-pressure combustion regimes for gasoline engines. This study analytically explores the fundamental thermodynamics of operation in these regimes under realistic burn duration, heat loss, boosting, and friction constraints. The intent is to identify the benefits of this approach and the path to achieving optimum engine and vehicle-level fuel economy. A simple engine/turbocharger model in GT-Power is used to perform a parametric study exploring the conditions for best engine efficiency. These conditions are found in the mid-dilution range, a result of the tradeoff between fluid property benefits of lean mixtures and friction benefits of higher loads. Dilution with exhaust gas is nearly as effective as air dilution when compared using a ‘fuel-to-charge’ equivalence ratio defined as $\Phi' \equiv \Phi(1-RGF)$ where RGF is the total residual gas fraction. Optimal brake efficiencies are obtained over a range $0.45 \leq \Phi' \leq 0.65$ for operation up to 3 bar manifold pressure, yielding peak temperatures under 2100 K and peak pressures under 150 bar. These conditions are intermediate between homogeneous charge compression ignition and spark-ignition regimes, and are the subject of much current research on advanced combustion modes. An engine–vehicle drive train simulation shows that accessing this thermodynamic sweet spot has the potential for vehicle fuel economy gains between 23% and 58%.

Keywords

Thermodynamics, fuel economy, high efficiency, gasoline, boosting, turbocharging

Date received: 13 March 2012; accepted: 13 June 2012

Introduction

The US Department of Energy (DOE) Vehicle Technologies Program has, as one of its key goals, to identify the ways to achieve 20–40% gain in light-duty (LD) engine peak efficiency, with 25% vehicle fuel economy improvement. To accomplish this for gasoline engines, several researchers^{1–3} have pointed out the potential advantages of dilute combustion, coupled with boosted, high-pressure operation, corresponding roughly to the best operating conditions for diesel engines.

These conditions in a gasoline engine have been beyond the traditional premixed combustion regime of spark ignition (SI). At greater than 30% dilution, either with air or EGR, flame propagation becomes too slow for reliable combustion; lower loads must be achieved by throttling with attendant pumping losses. In recent years, homogeneous charge compression ignition (HCCI) has been employed to achieve ultra-lean or

dilute combustion at low loads with dilution as high as 80%.⁴ As load is increased, and dilution is reduced below ~60%, the combustion becomes too rough and HCCI knock is encountered, or NOx limits are exceeded, thus forming an upper load limit for HCCI.^{5,6} As a result of these constraints, there remains a gap, between ~30% and 60% dilution, in which it has been difficult to operate. It has become common to refer to combustion in this regime as ‘advanced combustion’.

Attempts to access the advanced combustion regime from the high-load side have been moderately

Department of Mechanical Engineering, University of Michigan, USA

Corresponding author:

George A Lavoie, Department of Mechanical Engineering, University of Michigan, 1004 Walter E Lay Automotive Laboratory, 1231 Beal Avenue, Ann Arbor, MI 48109-2133, USA.
Email: glavoie@umich.edu

successful. Increased use of EGR in heavy-duty (HD), SI stationary natural gas engines have enabled brake efficiencies as high as 47%, with very low NOx emissions.⁷ Researchers at Southwest Research Institute (SwRI) have developed a new ignition system^{8,9} that extends the lean limit with potential to facilitate the application of dilute operation to LD engines in the context of the high-efficiency dilute gasoline engine (HEDGE) concept.⁸ Other ignition concepts are also being considered including a microwave-assisted spark plug.¹⁰ Stratified charge has been another major approach to achieve advanced combustion in SI gasoline engines.¹¹ The concept is to reduce the stratification relative to diesel combustion and avoid particulate emissions, while still providing enough local rich mixture to ensure ignition. Early attempts at SI, single-injection, direct-injection engines were successful in terms of fuel efficiency, but NOx emissions remained high, due to near-stoichiometric regions in the charge. Later use of multiple injection strategies showed improved results but still require NOx aftertreatment.¹²

Other techniques have approached the advanced combustion regime from the low-load side, concentrating on reducing the rate of heat release by thermal stratification,^{13,14} and by partial fuel stratification.^{15,16} A dual-fuel concept¹⁷ has also been used. In this approach, the main charge consists of premixed gasoline-air, with a small injection of diesel fuel to control ignition late in the compression stroke. As noted above, the key challenge to any fuel stratification method is the increased NOx and particulate emissions that result from the relatively rich regions of the charge.

Finally, spark assisted compression ignition (SACI) is an approach that, in principle, can access all regions of the advanced combustion regime from HCCI to SI.^{18–21} This concept relies on an SI flame to consume a portion of the charge before the main auto-ignition event occurs. This moderates the heat release and at the same time provides some control over combustion phasing.

In addition to the potential benefits of advanced combustion modes, boosted pressure-charged operation, either by turbochargers or by superchargers, can provide additional fuel economy benefits. For the engine, the benefit of boosting results primarily from the diminished relative importance of friction compared to output as the engine load is increased. At the same time, the turbine itself can provide additional work output depending on the enthalpy of the exhaust stream. Boosting technology is now appearing in the automotive marketplace with SI, stoichiometric operating strategies, and with limited EGR dilution. The question naturally arises: what is the benefit of applying both boosting and advanced combustion technologies, and how best can the technologies be employed?

Thermodynamic models have been used to explore some of the alternatives. Caton¹ presented a ‘walk-through’ of engine design and operating conditions leading from a current SI engine to an improved

concept that provided increased efficiency at two engine load conditions. The model results explained the significant potential gains relative to conventional engines that could be achieved by operating lean, with high EGR, high compression ratios and high pressure. Chadwell et al.²² used a similar thermodynamic modeling approach to explore the potential of four advanced combustion engine concepts relative to conventional diesel. Heat-release rates were taken from experimental data, and the operating range of each concept at maximum load was explored over a range of EGR rates and turbocharger efficiencies. Although efficiency gains were possible relative to current gasoline engines, the study concluded that none of the concepts were able to exceed the brake efficiency of the traditional lean burn diesel equipped with 90% effective NOx aftertreatment. Second-law analyses have also been carried out by Caton²³ and Farrell et al.²⁴ These studies included the loss of availability or exergy during the combustion process. The major effects on exergy loss were found to relate to combustion temperatures and heat transfer. Teh et al.^{25,26} carried out an adiabatic general second-law analysis of automotive engine cycles covering energy-release rate, volume ratio, and dilution by air or EGR. For a given fuel and oxidizer, these analyses confirm the efficiency benefit of lean or dilute, low-temperature engine operation.

The objective of the current work is to further explore the role of thermodynamic engine conditions in enabling high-efficiency engines, in particular to look at the tradeoffs between engine thermodynamics, the application of turbochargers, and downsizing. The intent is to provide a general framework to facilitate the evaluation of HCCI, SI, and advanced combustion modes in the context of engine-turbocharger technologies currently available.

The approach is to use GT-Power^{27,28} to simulate an idealized engine and turbocharger with a simple but appropriate level of complexity and assume optimal combustion is possible at all conditions. An ideal turbocharger representation is used, characterized by a specified efficiency. The idea is to identify the thermodynamic optimal conditions independent of the combustion constraints, which can be addressed in future work. Finally, we simulate an engine based on the optimal strategy, and apply it to a drive cycle with MATLAB-Simulink to estimate vehicle fuel economy improvements.

Model formulation

Figure 1 is a schematic of the single-cylinder engine represented by the GT-Power simulation with engine specifications given in Table 1. The engine specifications are chosen to represent a high compression ratio (12:1), LD, four-valve, gasoline direct-injection engine with four-cylinder displacement of 2.54 l. Valve timing is conventional, except for some calculations when an

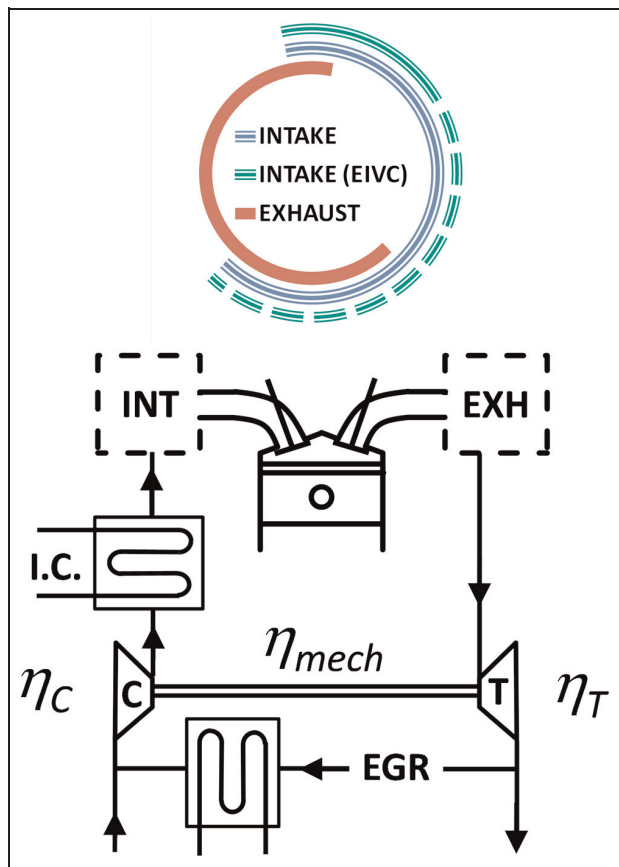


Figure 1. Schematic of engine model configuration.

Table I. Engine specifications.

Bore/stroke	90 mm/100 mm
Compression Ratio (CR)	12
Intake valves (2)	32.4 mm diameter / 10.7 mm lift – 12° ATC gas exchange
IVO (open at 0 lift)	60–224° ATC gas exchange
IVC (close at 0 lift)	26.1 mm diameter / 10.7 mm lift
Exhaust valves (2)	135° ATC firing
EVO (open at 0 lift)	371° ATC firing
EVC (close at 0 lift)	

ideal early intake valve closing was considered as a throttling strategy. In this case, the intake valve closing time was varied while the intake opening time remained fixed. The engine communicates with intake and exhaust plenums through short runners to minimize flow dynamics. Fuel is vaporized and mixed with the air during the intake process. Backpressures downstream of the turbine were assumed to be zero.

Turbocharger model

The ideal turbocharger system is characterized by specified efficiencies for the turbine η_T , the compressor η_C , and the mechanical link between them η_{MECH} . With efficiencies defining the ratio of actual work to isentropic expansion or compression work, an expression

relating the required exhaust pressure P_{EX} , to the desired intake pressure P_{IN} , can be written as

$$\left[1 - \left(\frac{P_{ATM}}{P_{EX}} \right)^{\frac{\gamma_T-1}{\gamma_T}} \right] = \frac{\dot{m}_C C_{PT} T_{ATM}}{\dot{m}_T C_{PT} T_{EX}} \frac{1}{\eta_{OTC}} \left[\left(\frac{P_{IN}}{P_{ATM}} \right)^{\frac{\gamma_C-1}{\gamma_C}} - 1 \right] \quad (1)$$

This equation reflects the energy balance between the work produced by the turbine with the work needed to operate the compressor, subject to the losses specified by the overall turbocharger efficiency η_{OTC} , which is defined as the product of the three efficiencies

$$\eta_{OTC} = \eta_T \eta_{MECH} \eta_C \quad (2)$$

Other terms in the equation are: ratios of specific heats γ , mass flows \dot{m} , and specific heats C_P , with subscripts T and C referring to turbine and compressor conditions, respectively. Atmospheric pressure and temperature are P_{ATM} and T_{ATM} . Details of this formulation can be found in Watson and Janota.²⁹ On the right-hand side of equation (1), exhaust temperature and overall turbocharger efficiency appear in the denominator so that higher values of either will decrease the required backpressure and reduce the pumping work of the engine for a given P_{IN} . The configuration shown in Figure 1 is for a low-pressure EGR loop, and the fluid properties of the compressor take the composition into account. With the ideal turbocharger representation of equation (1), the results will also be representative of a high-pressure EGR loop provided the overall turbocharger efficiency is adjusted to take compressor composition and size into account, and there is enough backpressure to drive the flow. The details of the turbocharger losses and configuration are indirectly taken into account by the overall turbocharger efficiency. The heat exchangers shown in Figure 1 are used to maintain the compressor inlet temperature at T_{ATM} and the engine intake temperature at T_{IN} .

Burn rate, heat transfer, and friction

Table 2 lists the submodels and related assumptions used. The calculations employ the standard Woschni correlation³⁰ for heat transfer with GT-Power default coefficients. Heat release is described by the Wiebe function

$$x_b = 1 - \exp \left[-a \left(\frac{\theta - \theta_0}{\Delta\theta} \right)^{w+1} \right] \quad (3)$$

where $\Delta\theta$ and θ_0 are set by matching the desired 10–90% burn duration, and crank angle at 50% burn, CA50, with efficiency factor $a = 5$ and shape parameter $w = 2$ taken from Heywood.³¹ Combustion efficiency is taken to be 100%.

Table 2. Submodel specifications.

Heat transfer	Standard Woschni ^{27,30}
Heat release	Standard Wiebe ³¹
Friction	Chen–Flynn ^{27,32}
NOx model	Two-zone Zeldovich ^{27,31}

Table 3. Operating conditions and parameters.

r/min	2400 ($U_P = 8 \text{ m/s}$)
Φ	0.2–1.2
EGR	0–80%
P_{EX}	1–3 (bar)
T_{IN}	333 K (60°C)
T_{ATM}	298 K (25°C)
T_{WALL} (K)	460 (head), 510 (piston), 390 (cylinder)
T/C Eff (η_{OTC})	40, 50, 60%
Burn 10–90	25° CA
CA50	10° ATC (~max efficiency)

Friction is described by the Chen–Flynn expression³² modified to include a quadratic piston velocity term

$$\text{FMEP (bar)} = 0.4 + 0.005P_{MAX} + 0.09U_P + 0.0009U_P^2 \quad (4)$$

where FMEP is the friction mean effective pressure, P_{MAX} is the maximum cylinder pressure in bar, and U_P is the mean piston speed in m/s. Equation (4) has GT-Power recommended parameters and follows closely the friction curves shown in Heywood.³¹ Other more detailed friction models exist.^{33–37} These are more complex and deal explicitly with aspects of engine design; however, for consideration of a single engine, the simpler expression is more convenient and retains the most important feature, namely that friction increases with engine load (reflected in peak pressure), but not in direct proportion. Calculations of NOx formation are carried out using the three-reaction Zeldovich mechanism³¹ and GT-Power's two-zone combustion model.

Operating conditions

Table 3 lists the operating conditions and model parameters used in the calculations. Engine speed was set at 2400 r/min, corresponding to the location of best fuel economy for a modern LD engine,³⁸ where mean piston speed $U_P = 8 \text{ m/s}$ for the chosen engine stroke of 100 mm. Fuel air equivalence ratio, Φ , ranges from rich at 1.2 to very lean at 0.2, while $\Phi = 1$ operation with EGR up to 80% corresponds to approximately the same range of dilution as with air. Intake pressures up to 3 bar absolute are considered, with an intake temperature of 60°C. The inlet to the compressor is held at 25°C. This is realistic for air dilution or for EGR with the high-pressure loop, but may be low for EGR in a low-pressure loop; in this case, the turbocharger effectiveness will be overestimated somewhat in the

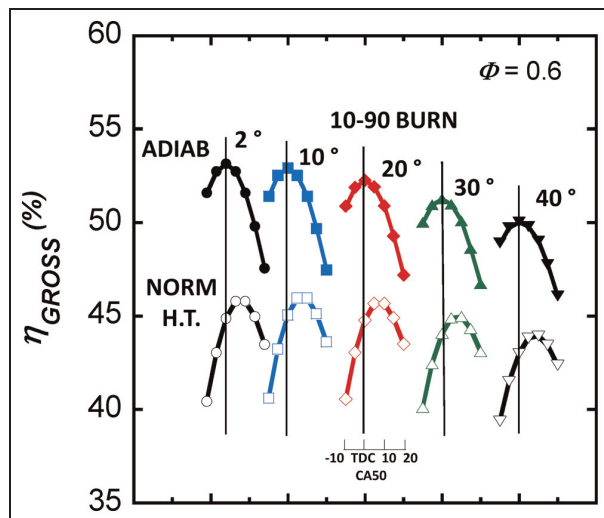


Figure 2. Effect of burn duration, timing, and heat transfer on gross indicated efficiency.

calculations. Combustion chamber wall temperatures were fixed for piston, head, and cylinder at 510 K, 460 K, and 390 K respectively, values chosen to represent a mid-load condition and determined by scaling experimental data from Heywood³¹ and Cho et al.³⁹ according to engine power. Calculations were carried out with variable wall temperatures, but the effect on efficiency was minimal. Similarly, wall temperatures for intake runner and port were set at 350 K and 450 K, respectively, and exhaust runner and port were 600 K and 550 K. Turbocharger efficiencies of 40, 50, and 60% were considered.

Of particular importance is the choice of combustion duration and phasing. Figure 2 shows a parametric study of the effect of these variables on gross efficiency with and without heat transfer for equivalence ratio 0.6. Each seven-point curve represents a timing sweep of CA50 from –10 to + 20° ATC at 5° intervals for a particular 10–90% combustion duration. Five such sweeps are shown with normal heat transfer and five with heat transfer set to zero. Combustion durations range from 2°, characteristic of ideal constant volume cycle calculations to 40°, representative of a slow dilute burning SI engine. For the adiabatic sweeps, the best efficiency occurs for a symmetric burn with CA50 at top dead center (TDC). Retarded combustion always incurs a penalty. With normal heat transfer, the optimal CA50 is ~ 10° ATC, the result of a tradeoff between heat losses for early high-temperature conditions, and expansion losses for late combustion. Further, there is little efficiency penalty for a longer burn duration up to 20°. Similar results are found for $\Phi = 0.2$ and $\Phi = 1.0$. For all equivalence ratios, the optimal CA50 decreases to ~ 5–7° ATC as the 10–90% burn duration decreases, but with minimal effect on efficiency relative to a CA50 of 10° ATC, e.g. < 0.2% gain in gross efficiency. For this study, adiabatic cases used CA50 = 0° ATC, while for cases with heat transfer, the phasing was set at 10°

ATC. Combustion duration from 10–90% heat release was chosen to be 25°, midway between HCCI and dilute SI combustion. This choice is intended to identify the best possible efficiency over the range of conditions studied. Similar calculations were carried out with a relatively asymmetric burn curve that had a longer tail – the optimal CA50 was advanced, but the best efficiency was unchanged. In practice, constraints on maximum heat-release rates and flammability under certain operating conditions could prevent the engine from achieving the best efficiency. Consideration of these effects is important, but beyond the scope of the present study.

Naturally aspirated results

Effect of losses

Figure 3 demonstrates the effect of various losses on the overall engine efficiency as predicted by the model. A series of efficiency curves are plotted against equivalence ratio Φ for a naturally aspirated engine with parameters as noted in the subsection on operating conditions. The uppermost curve represents the best possible efficiency (gross) with adiabatic, nearly constant volume combustion (2° CA duration). As Φ approaches zero, this curve approximates the standard air-cycle efficiency, $\eta = 1 - 1/\text{CR}^{(\gamma-1)}$, which gives ~60% with CR = 12 and $\gamma = 1.367$ for air at an estimated average cycle temperature of 750K. As Φ increases, the efficiency falls due to decreasing γ as the added fuel and combustion products increase the specific heat. The curve drops rapidly for rich mixtures beyond $\Phi=1$ due to lack of complete conversion of fuel to CO₂ and H₂O.

The series of lower efficiency curves in Figure 3 is the result of successively introducing losses due to

combustion duration (25° CA duration), heat transfer, pumping (net efficiency), and finally friction losses, leading to the final brake efficiency. Under these engine operating conditions, most of the losses are due to heat transfer and friction. At this speed and with equal intake and exhaust pressures, there is little pumping work. With the Woschni correlation used here, heat loss relative to the total fuel energy remains nearly constant over the range of equivalence ratios. As noted by Caton,⁴⁰ there are many heat-transfer correlations in the literature that predict different heat-loss values and have somewhat different forms. For example, the Hohenberg⁴¹ correlation for the heat-transfer coefficient does not contain a combustion-derived velocity term as does the Woschni correlation. For this reason, calculations using the Hohenberg correlation show an increase in heat-transfer losses as the mixture is leaned out and result in a flatter gross efficiency curve than that shown in Figure 3. In addition, there is evidence that ultra-lean, HCCI combustion may have lower heat transfer,⁴² suggesting that heat transfer is dependent on combustion mode. While these aspects of heat transfer are important, they are beyond the scope of this study. In addition, for typical levels of heat losses, i.e. ~20% of fuel energy, a large relative change in heat transfer has only a moderate effect on efficiency, and so we expect the trends to be valid, regardless of the heat-transfer correlation used.

As shown in Figure 3, friction losses become important at low loads, and at lean enough conditions, completely outweigh the benefits of lean operation seen on an indicated basis. The reason for this is evident in equation (4) where the FMEP does not decrease proportionally with peak pressure (and load), and thus becomes a dominant factor with lean operation. The final result is a brake efficiency curve that is low for very lean mixtures, and rises to a maximum in the mid-load range, and then falls again as the mixture becomes fuel rich.

Dilution method

Many advanced combustion concepts employ large quantities of hot residual gas as diluent. This has advantages over air dilution because NO emissions are generally lower for an EGR diluted mixture and after-treatment is facilitated by overall stoichiometric operation. These two dilution methods can best be compared by introducing the ‘fuel-to-charge’ equivalence ratio Φ' defined by

$$\begin{aligned}\Phi' &\equiv \frac{F/(A+R)}{(F/A)_{\text{ST}}} \\ &= \frac{\Phi(1-\text{RGF})}{[1 + \Phi \cdot \text{RGF} \cdot (F/A)_{\text{ST}}]} \cong \Phi(1-\text{RGF})\end{aligned}\quad (5)$$

where F , A , and R denote mass of fuel, air, and residual gas, RGF is the total residual gas fraction and subscript ST refers to a stoichiometric mixture. (The

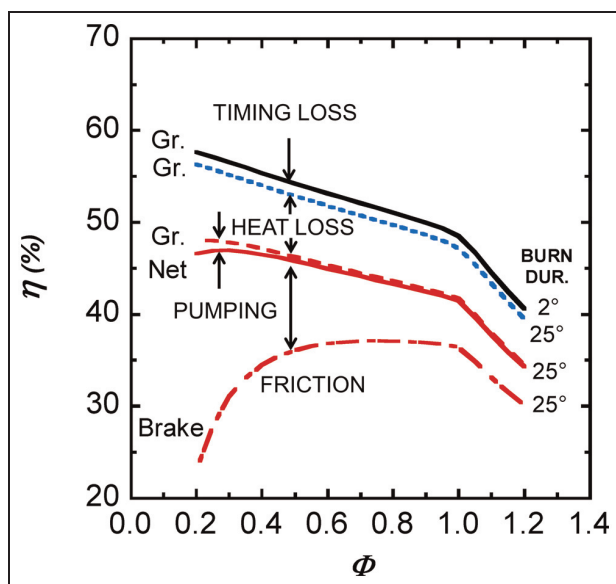


Figure 3. Key efficiency losses as a function of equivalence ratio.

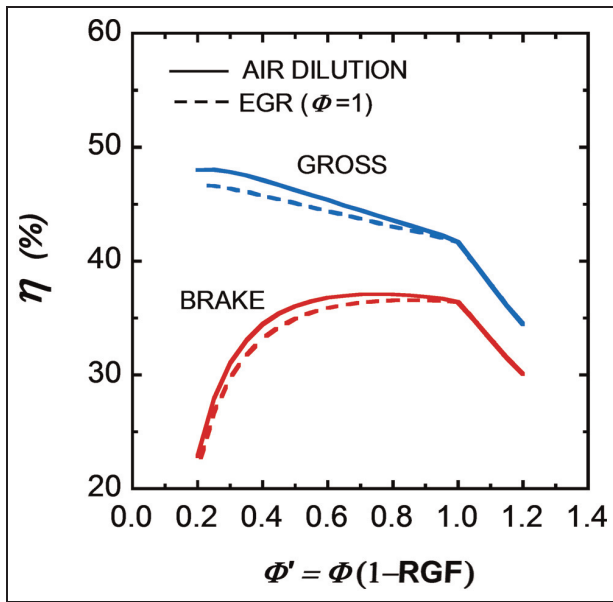


Figure 4. Diluent effect on efficiency as a function of the 'fuel-to-charge' equivalence ratio, Φ' . EGR versus air dilution.

approximation holds because the stoichiometric fuel-air ratio is ~ 0.06 , resulting in a denominator close to 1). Φ' is a measure of the specific energy content of the charge and is a rough indicator of the temperature increase due to combustion and for a given manifold pressure, is approximately proportional to engine load.

RGF may be made up of internal and external residual gas so that

$$(1 - \text{RGF}) = (1 - f_{\text{RES}})(1 - f_{\text{EGR}}) \quad (6)$$

where f_{RES} is the fraction of burned gas, expressed as a fraction of the total cylinder contents, which does not recirculate externally, while f_{EGR} refers to the fraction of residual gas entering through the intake manifold, specified relative to that portion of the charge supplied by the manifold. Note that for the modeled engine, the residual fraction is small so that RGF is approximately equal to the EGR fraction. (Equation (6) assumes the fuel is premixed in the manifold; for a gasoline direct injection gasoline direct injection (GDI) engine, the effective EGR fraction must be adjusted by the fraction of fuel mass relative to the intake mass, which will be less than $\Phi(F/A)_{\text{ST}}$ or $\sim 7\%$).

Figure 4 compares air and residual gas dilution in terms of gross and brake efficiencies plotted against Φ' . In the case of dilution with residual gas, the equivalence ratio is held fixed at $\Phi = 1$. The residual gas dilution gives slightly lower efficiencies, but overall, the curves are similar. In both cases, dilution is advantageous, partly from the change in composition, and partly from the decrease in burned gas temperature. In the case of unburned mixtures, increased dilution reduces the effect of the high C_P fuel with either air or EGR dilution. For burned mixtures diluted with air, dilution reduces the fraction of high C_P combustion products (CO_2 and H_2O). For burned mixtures diluted with either air or

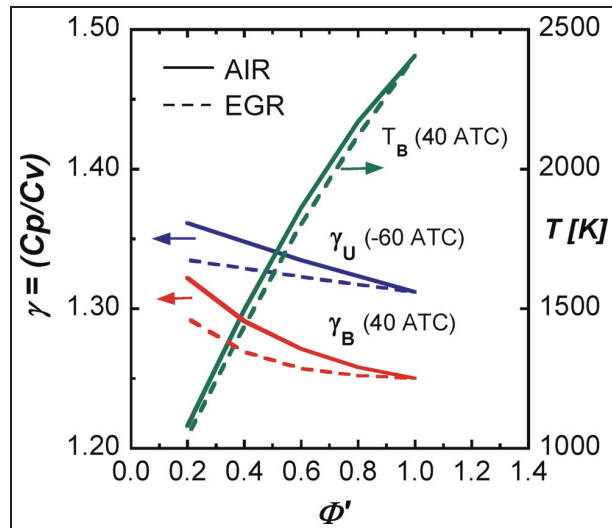


Figure 5. Diluent effect on unburned and burned gas specific heat ratios γ_U and γ_B , and burned gas temperature T_B as a function of Φ' . Burned gas properties evaluated at 40° ATC; unburned at -60° ATC. EGR versus air dilution.

residual gas, the decrease in burned gas temperature adds an additional reduction in C_P . Figure 5 shows the resulting effect on burned and unburned γ values corresponding to Figure 4. The figure shows the temperature T_B at which the burned properties were evaluated (40° ATC) for both air and EGR dilution. Unburned properties were evaluated at -60° ATC where the temperature was 520 ± 10 K for all conditions. The result is that both unburned and burned gas γ values increase with dilution; the effect is seen to be greater for air compared to residual gas. The ratio of γ for EGR dilution versus air dilution decreases by about 2% as the mixture is leaned out, in rough agreement with the small falloff in gross efficiency for EGR versus air dilution. Note that the difference in burned gas temperature between air and residual gas dilution is small at a given dilution level and only has a minimal effect.

Load control

The resulting efficiency effects are seen in Figure 6 where four methods of load control are compared for a naturally aspirated engine: dilution with air, dilution of a $\Phi = 1$ mixture with residual gas, and a stoichiometric mixture modulated by throttling and by early intake valve closing (EIVC). The sharp drop in efficiency at high loads in all cases is due to the inclusion of rich conditions beyond stoichiometric. For both the air and residual gas dilution cases, the gross efficiency increases with decreasing load, while for throttling and EIVC, the curves remain flat or decrease slightly. This is a result of the behavior of peak cycle temperature shown in Figure 7, where both air and EGR dilution cases have declining temperatures at lower loads, while the throttling and EIVC cases maintain high peak temperatures because these latter load control methods do not

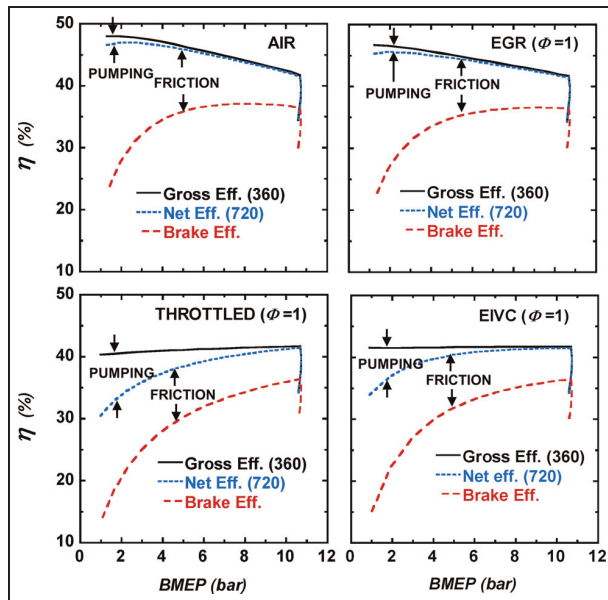


Figure 6. Comparison of various means of load control showing the effect of changes in properties on the slope of gross efficiency curves; and of changes in pumping losses on net efficiency. Sharp drop in efficiency curves at high load occurs when mixture is rich at $\Phi \geq 1$.

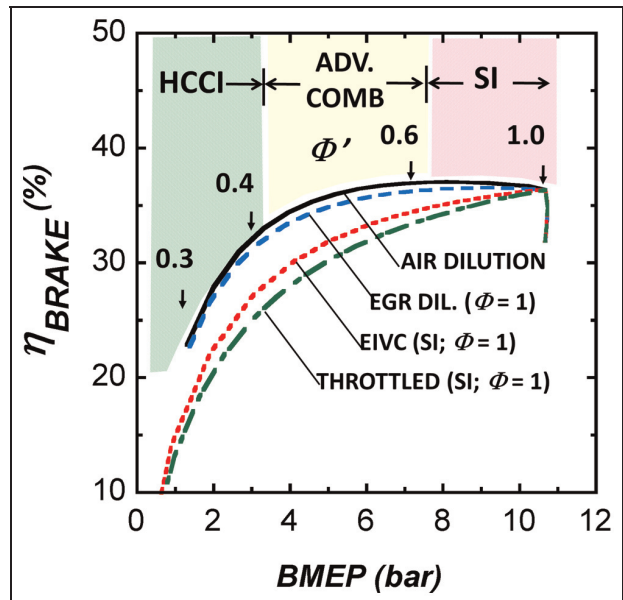


Figure 8. Potential for brake efficiency gains for naturally aspirated engines, depending on combustion regime: HCCI, advanced combustion, and SI.

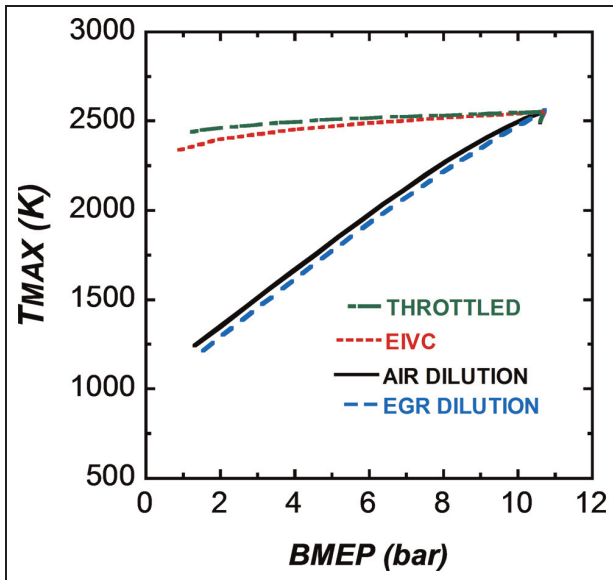


Figure 7. Peak cycle temperatures for various load control methods.

involve significant dilution. Figure 6 shows that EIVC incurs some pumping loss, but not as much as the pure throttling case. Comparing brake efficiency, we see that for both air and residual gas dilution, overall efficiency rises or remains flat over a substantial part of the load range, while throttling and EIVC show steady declines as load decreases.

Figure 8 compares the brake efficiency for the four naturally aspirated load control methods as a function of load. For reference, an approximate scale of Φ' is

indicated in the upper part of the figure as it applies to the two dilution cases. It is divided into ranges of combustion mode based on current experiments reported in the literature: HCCI ($0.3 \leq \Phi < 0.45$); advanced combustion ($0.45 \leq \Phi < 0.65$); and conventional SI ($0.65 \leq \Phi < 1.0$). At the lowest loads, HCCI can be seen to provide significant gains relative to throttling and EIVC. Further gains are possible at mid-loads by use of advance combustion, e.g. SACI, or stratified charge.

Validation

Comparing with measured brake efficiency is difficult because of the variations in hardware and accessory loading assumptions. Nevertheless, the predicted 36–37% peak brake efficiency values (brake specific fuel consumption, BSFC ~ 225 g/kWh) shown in Figures 6 and 8, for stoichiometric SI engines are consistent with those achieved by current naturally aspirated, LD, high compression ratio engines.⁴³ For a more critical test related to thermodynamic effects, it is convenient to look at gross thermodynamic efficiency. Figure 9 compares measured gross thermodynamic efficiency to the model predictions of Figure 8, for air dilution, EGR dilution, and throttling as load control methods, plotted as a function of gross indicated load (GMEP). The experimental results were obtained as part of experiments on the University of Michigan (UM) fully flexible valve actuation engine¹⁸ with CR = 12.4 at 2000 r/min. Data for three combustion modes are shown: HCCI, SACI, and throttled SI. An additional experimental data point is included from Caris and Nelson⁴⁴ obtained for unthrottled SI best fuel economy

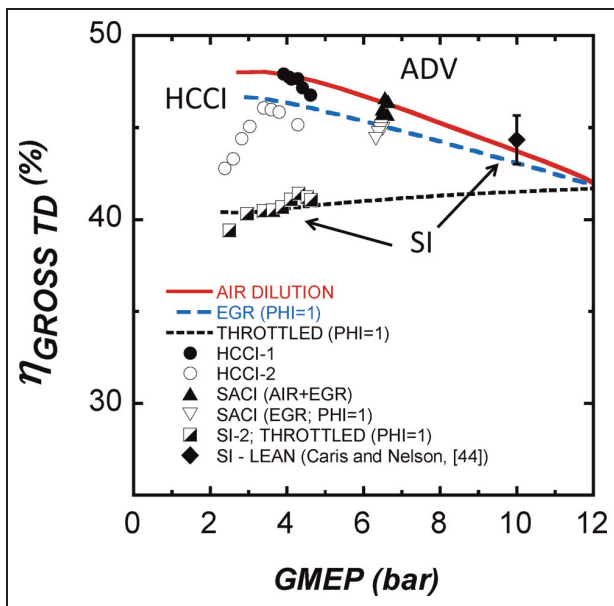


Figure 9. Comparison of predicted gross thermodynamic efficiency and experimental values versus GMEP for three combustion modes: HCCI, advanced combustion (SACI), and SI, both lean unthrottled (Caris and Nelson,⁴⁴) and stoichiometric throttled (SI-2). Thermodynamic efficiency compensated for incomplete combustion.

operation ($\Phi \sim 0.9$) at 12:1 compression ratio, also at 2000 r/min. All data points have been corrected to 100% combustion efficiency to match the modeled assumptions.

For the most part, the model is in good agreement with the experiments, and confirms the relative thermodynamic benefit of dilute mixtures compared to throttling. This effect is due to mixture properties since pumping losses do not directly affect gross efficiency. Except for a rapid efficiency falloff for the lowest load HCCI points, the model is within $\pm 3\%$ of the experiments. Caton⁴⁰ has shown that the choice of heat-transfer model can affect predicted efficiencies by $\pm 5\%$, and with a typical experimental error of $\pm 3\%$ (indicated by the error bar on the single SI point), the absolute agreement in the figure may be somewhat fortuitous. Nevertheless, the relative behavior of the model follows the experiments well, except for the low-load region. Thermodynamic analysis of the HCCI data points in the low-load region reveals that the decrease in efficiency is likely due to increasing gas temperatures provided by internal EGR in the negative valve overlap controlled engine. These temperatures cause a decrease in specific heat ratio and cycle efficiency. At the leanest points, increased relative heat transfer may also play a role.

Turbocharged results

Perfect boosting

Two efficiency benefits of operating an engine at high pressure can be seen in Figure 10, where the special case

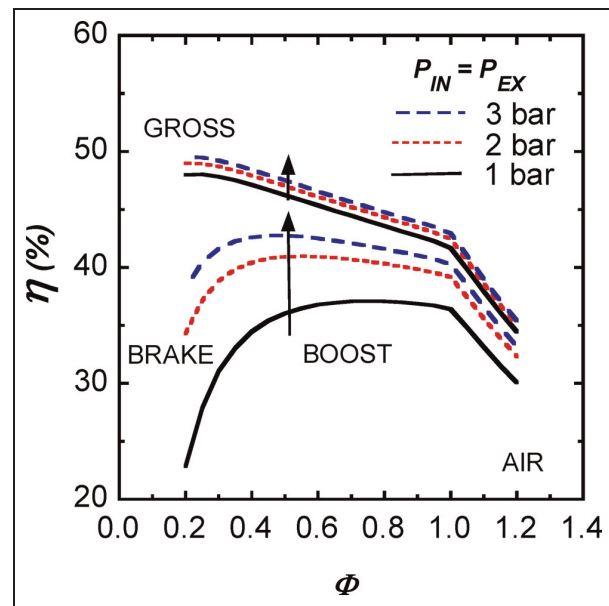


Figure 10. Gross and brake efficiencies versus equivalence ratio for 'perfect' boosting with $P_{IN} = P_{EX}$. The figure shows the effect of reduced relative heat transfer on gross efficiency at higher pressure, and resulting reduced friction losses at the corresponding higher loads.

of 'equal' boosting (intake pressure the same as exhaust pressure) is considered for intake and exhaust pressures of 1, 2, and 3 bar. The graph plots gross and brake efficiency versus Φ for air diluted mixtures. The upper three curves show gross efficiency and demonstrate a small increase as pressure is raised. This is due to the reduced effect of heat transfer for the higher pressure case. Heat transfer in engines can be described in general by the following expression relating Nusselt number to Reynolds number

$$Nu = \frac{hB}{\kappa} \propto Re^m \quad (7)$$

where h is the heat-transfer coefficient, B is the cylinder bore and κ is the thermal conductivity. Reynolds number is $Re \equiv \frac{\rho U_P B}{\mu}$ with density ρ , mean piston speed U_P and viscosity μ , and the Reynolds number exponent $m \sim 0.8$.³¹ This general scaling behavior is exhibited by many empirical correlations for the engine heat-transfer coefficient, including the Woschni correlation used here. As density is increased, the total mass in the charge increases, while the heat-transfer coefficient also increases, but not as fast. For a given temperature driving force, a measure of the effect of heat transfer on the gas is given by the Stanton number, St

$$St \equiv \frac{h}{\rho C_P U_P} = \frac{Nu}{Re \cdot Pr} \propto Re^{-(1-m)} \quad (8)$$

which decreases as Reynolds number increases since the Reynolds number exponent is less than 1. (Since Prandtl number $Pr \equiv \frac{C_P}{\kappa}$ is close to unity for air and

combustion gases, the scaling effect of this term is minimal and is ignored). The Reynolds number increases with boost due to increasing charge density. This factor is also part of the reason large bore engines are generally more efficient; in this case, Reynolds number increases due to increasing bore size. Velocities scale with piston speed, which tends to remain relatively constant for all engines.

Also shown in Figure 10 is the much larger beneficial effect of boost pressure on brake efficiency. This is because friction does not increase in direct proportion to density or peak pressure (see equation (4)); thus, as pressure and load increase, the parasitic friction loss becomes less and less important. Furthermore, for the highly boosted cases, the position for maximum brake efficiency moves to leaner mixtures.

Ideal boosting

Figures 11 and 12 demonstrate the third beneficial effect of turbocharging, i.e. due to the turbocharger itself, which provides additional work if the exhaust temperature is high enough. Figure 11 shows the ‘equal pressure’ ($P_{IN} = P_{EX} = 2$ bar) brake efficiency curve for air dilution from Figure 10 plotted against Φ , along with three additional simulations, also with 2 bar inlet pressure, but with exhaust pressure determined from the ‘ideal’ turbocharger equations (1) and (2). The overall turbocharger efficiencies shown are: 40%, typical of current automotive turbochargers; 50%, representing improved automotive turbochargers; and 60%, reflecting a future high-performance turbocharger comparable to large-scale marine engine technology. At the higher equivalence ratios, all of the turbocharger simulations give higher efficiency than the equal pressure

case; and the higher the turbocharger efficiency, the greater the effect. At higher equivalence ratios, the higher exhaust temperature (and enthalpy) permits the turbine to extract enough work to provide the desired inlet pressure at an exhaust pressure below the inlet pressure, requiring negative pumping work. The opposite is true for the leanest mixtures. In this case, the back pressure required (see equation (1)) must be higher than the inlet pressure so that the pumping work is positive and brake efficiency is decreased. This is shown in Figure 12 where the corresponding curves for pumping work are displayed.

Optimal boost strategy

Figure 13 shows a series of brake efficiency curves like those in Figure 11, but for one turbocharger efficiency of 50% at different inlet pressures and plotted as a function of brake load. Each curve spans a range of Φ from 0.2 to 1.2. As inlet pressure increases, the corresponding load range shifts upward until at the highest boost level of 3 bar absolute, the peak load reaches 37 bar. Each curve begins with low brake efficiency at the leanest conditions, and then rises to a maximum. The efficiency then decreases slowly as the mixture is enriched and stoichiometric conditions are reached, due to the thermodynamic tradeoffs noted earlier; the vertical drop in efficiency at the highest loads is due to operation beyond $\Phi = 1$.

Considering all the curves it can be seen that for a given brake load there is an optimal inlet pressure and Φ for best efficiency. Connecting these points produces the upper envelope of curves, shown as a heavy line. Along the line are marked the optimal values of Φ' which increase as boost is increased. (Although the

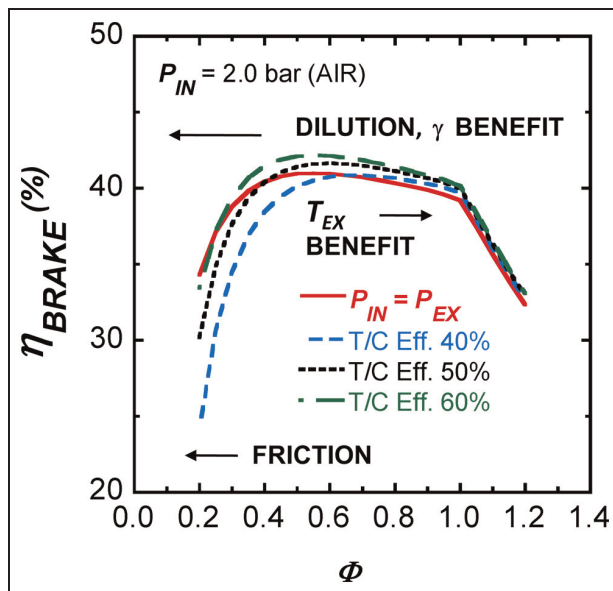


Figure 11. Effect of ideal boosting on brake efficiency for three turbocharger efficiencies relative to ‘perfect’ boosting ($P_{IN} = P_{EX}$), showing tradeoffs between the benefits of dilution and exhaust temperature.

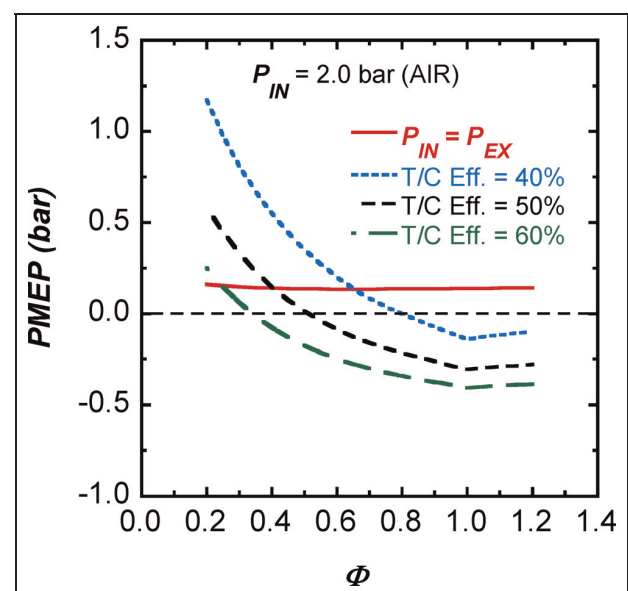


Figure 12. Effect of ideal boosting on pumping work for three turbocharger efficiencies compared to ‘perfect’ boosting ($P_{IN} = P_{EX}$).

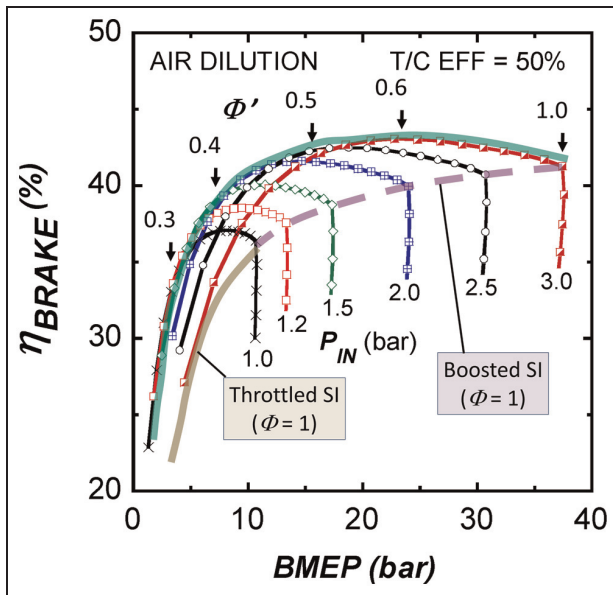


Figure 13. Family of brake efficiency curves for various intake pressures at a turbocharger efficiency of 50% for air dilute operation. Upper envelope indicates optimal boosting strategy with Φ' increasing as pressure level increases. Solid lower curve shows efficiency for stoichiometric throttled operation, while dashed curve shows efficiency for boosted stoichiometric conditions.

curves in this figure are for air dilution, the generalized Φ' metric defined in equation (5) is used for later comparison with EGR results. Connecting the $\Phi = 1$ points on each curve in Figure 13 corresponds to a boosted conventional SI engine with no EGR, shown as the lower heavy dashed line. The lower solid portion of this curve represents the throttled SI curve previously shown in Figure 8. The two heavy lines indicate the upper and lower limits between stoichiometric, undiluted operation, and air dilute operation. The figure shows the clear efficiency benefit of boosting and the additional advantage of dilution. These results are thermodynamically consistent with current boosted diesel and large gas engine practice where equivalence ratios at best efficiency are in the 0.5–0.6 range.

Figure 14 shows Φ' and P_{IN} along with the pumping work pump mean effective pressure (PMEP), plotted as a function of brake mean effective pressure (BMEP) for the optimal air dilute strategy of Figure 13. At the lowest loads, there is not enough enthalpy in the exhaust to produce any significant benefit from turbocharging, and P_{IN} remains near 1 bar up to $\Phi' \sim 0.3$ and a BMEP of ~ 4 bar. Beyond this point, both Φ' and P_{IN} increase together until the maximum inlet pressure of 3.0 bar is reached at about 20 bar BMEP. Pumping work remains slightly positive. Beyond this point, additional load can only be achieved by increasing Φ' so that the pumping work decreases rapidly due to the higher exhaust temperature.

Figures 15 and 16 show the effect of turbocharger efficiency on the optimal strategy, again for air dilution.

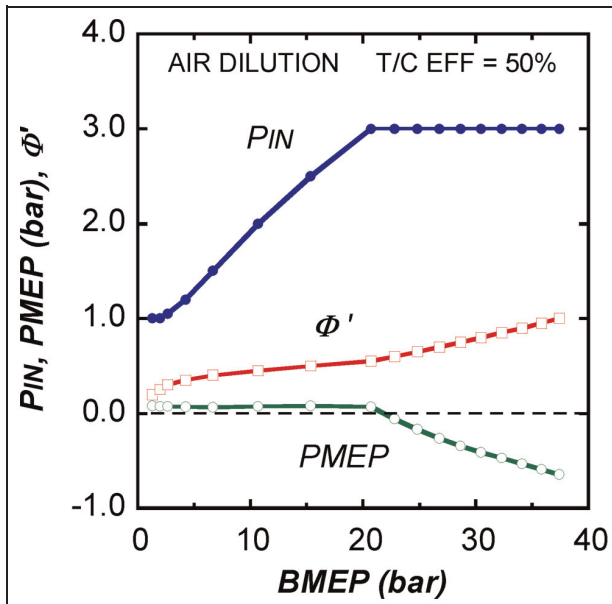


Figure 14. Intake pressure, Φ' and PMEP for optimal boosting strategy of Figure 12.

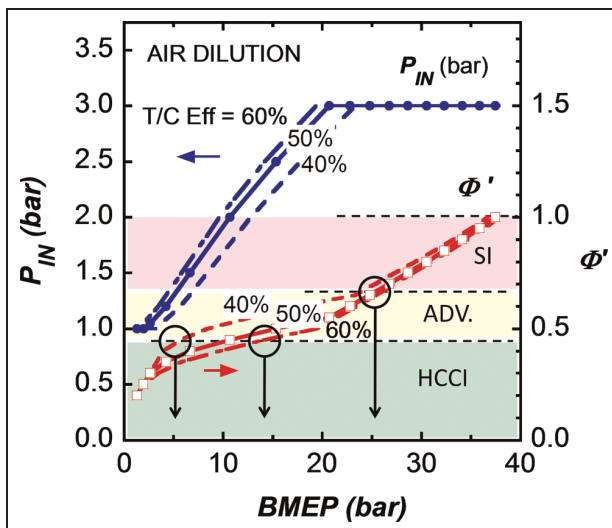


Figure 15. Effect of turbocharger efficiency on intake pressure and Φ' as a function of brake load for optimal boosting strategy. Higher turbocharger efficiency permits leaner operation at a given brake load, and also extends the range of HCCI operation defined by $\Phi' < 0.45$.

Figure 15 indicates Φ' and P_{IN} for three turbocharger efficiencies, 40%, 50%, and 60%, plotted as a function of brake load. The corresponding pumping work curves are shown in Figure 16. As expected, the higher turbocharger efficiency requires less pumping work over a wider range of load compared to the lower turbocharger efficiency, and for most of the range, its pumping work is negative. As can be seen from Figure 15, this enables higher intake pressures and lower equivalence ratios for a given brake load, with implications for the combustion mode limits.

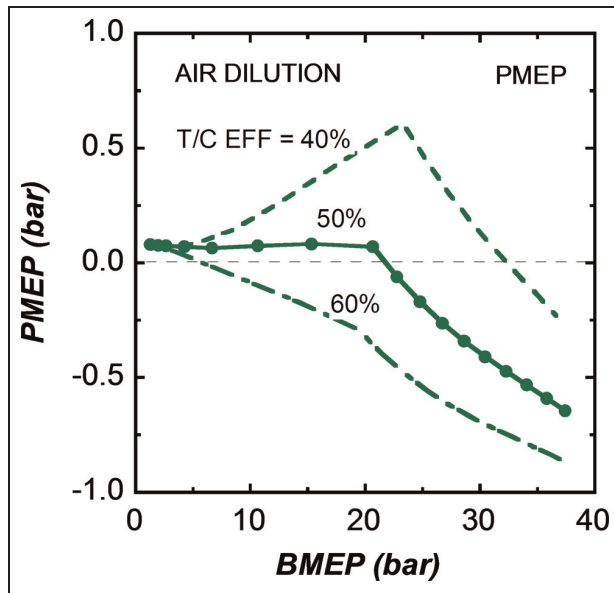


Figure 16. Effect of turbocharger efficiency on PMEP work as a function of brake load with optimal strategy. Turbocharger efficiency of 60% shows negative (beneficial) pumping work over most of the range while the lower efficiency of 40% requires positive work, except at the highest loads.

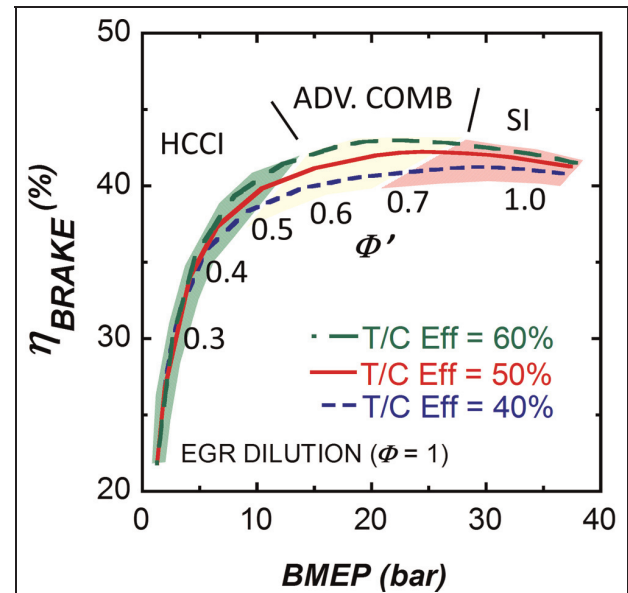


Figure 18. Optimal brake efficiency versus brake load for stoichiometric EGR dilution and three turbocharger efficiencies. Results are similar to air dilution. Combustion regions defined by Φ' transitions: HCCI–advanced ($\Phi'=0.45$); advanced–SI ($\Phi'=0.65$). Sloping boundaries between regions reflects the behavior in Figure 15.

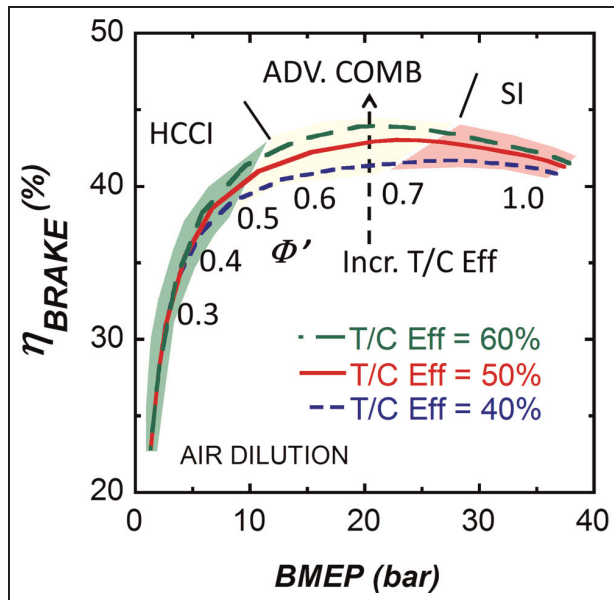


Figure 17. Optimal brake efficiency versus brake load for air dilution and three turbocharger efficiencies. Combustion regions defined by Φ' transitions: HCCI–advanced ($\Phi'=0.45$); advanced–SI ($\Phi'=0.65$). Sloping boundaries between regions reflects the behavior in Figure 15.

Also shown in Figure 15 are three horizontal bands corresponding to three modes of combustion: HCCI, advanced, and SI, with boundaries separating the modes at $\Phi' \sim 0.65$ for the SI flammability limit and $\Phi' \sim 0.45$ for the HCCI ringing limit. These boundaries

are not fundamental limits, but are approximate and based on experimental data for SI and HCCI engines. In particular, the HCCI limit is based on the data of Dec and Yang,⁴⁵ which shows a ringing index constrained maximum Φ' of ~ 0.45 up to about 3 bar intake pressure. Recently, Yang et al.⁴⁶ have shown that this limit depends on fuel type and intake temperature, and may go as high as $\Phi' \sim 0.55$. For the gasoline calculations here, the lower value is appropriate.

In Figure 15, it can be seen that as turbocharger efficiency increases from 40% to 60%, the HCCI limit of $\Phi \sim 0.45$ is reached for each curve at load points increasing from ~ 5 bar to ~ 14 bar BMEP. Thus, a turbocharger with 60% efficiency could potentially enable a boosted HCCI engine covering the entire load range of current naturally aspirated SI engines. With advanced combustion modes, this range could be pushed further to ~ 25 bar BMEP, without departing from the optimal fuel economy strategy.

EGR versus air dilution

Up to this point, the results shown have been for air dilution. As indicated earlier, EGR dilution is almost as beneficial. Figures 17 and 18 show the optimal brake efficiencies for air and EGR dilution, respectively, for turbocharger efficiencies of 40%, 50%, and 60%. Compared to air, EGR gives slightly lower overall maximum brake efficiencies, e.g. 43% versus 44% at 20 bar BMEP for the highest turbocharger efficiency. The

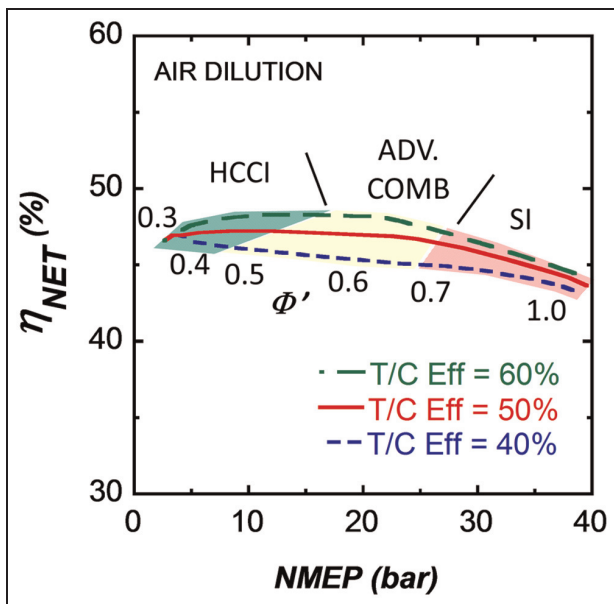


Figure 19. Effect of turbocharger efficiency on net efficiency at optimal conditions for air dilution.

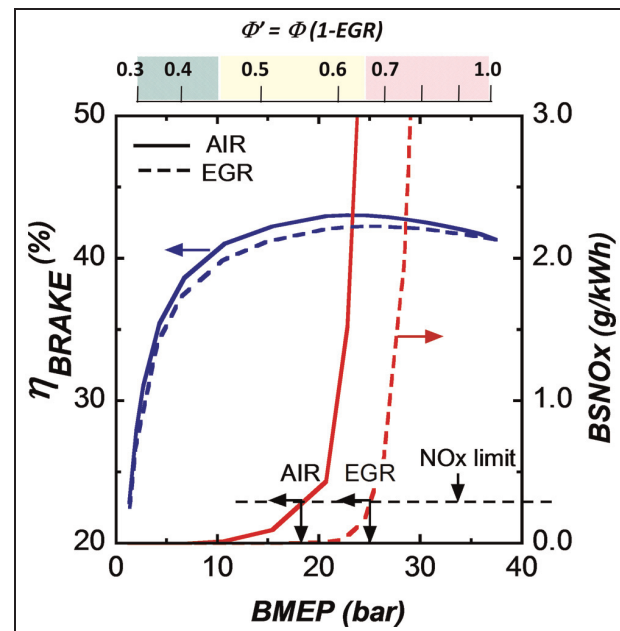


Figure 21. Predicted NOx emissions along the optimal boost curves for air and EGR dilution. Combustion regimes are shown by the Φ' scale at the top of the figure. Load limits are shown for emissions below 2010 EPA heavy-duty truck regulation of 0.26 g/kWh BSNOx emissions.

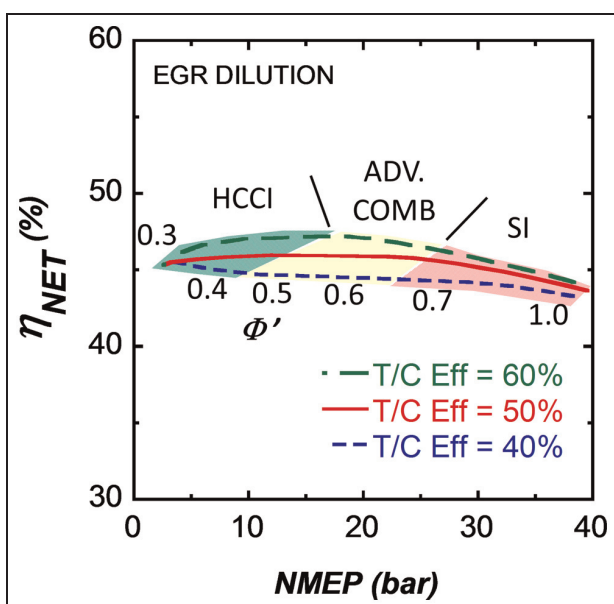


Figure 20. Effect of turbocharger efficiency on net efficiency at optimal conditions for stoichiometric EGR dilution.

bands overlying the curves indicate the three combustion regimes: HCCI, advanced, and SI, with regime transitions at $\Phi' \sim 0.45$ and 0.65 . The sloping boundaries result from the tradeoff between in-cylinder thermodynamic effects and turbocharger efficiencies, noted in the discussion of Figure 15.

Figures 19 and 20 show the corresponding net efficiency versus net mean effective pressure (NMEP) over the optimal strategy conditions for air and EGR, again for turbocharger efficiencies of 40%, 50%, and 60%. In the mid-load range, there is a significant difference due

to turbocharger efficiency and its effect on pumping work. However, at both low and high loads, the effect diminishes. In the case of low loads, this is due to the fact that the exhaust enthalpy is too low for any of the turbochargers and boost is minimal. At high loads, the mixtures approach stoichiometric with higher exhaust temperature, and there is a decrease in γ for the gas entering the turbine with a resulting drop in energy recovered.

In addition to the useful efficiency effects of low-temperature combustion, NOx emissions can be expected to be low. Figure 21 plots efficiency and NOx versus BMEP for the case of 50% turbocharger efficiency. Across the top of the figure is an approximate scale of Φ' . As expected, NOx emissions are significantly lower for EGR dilution. Stoichiometric operation with EGR dilution could satisfy the 2010 Environmental Protection Agency (EPA) heavy duty truck BSNOx limit of 0.26 g/kWh up to 25 bar BMEP compared to about 18 bar for air dilution. The low NOx region is within the HCCI and advanced combustion region, i.e. $\Phi' < 0.65$. Note that these NOx projections are likely to be optimistic since operating in both HCCI with $\Phi' < 0.45$ and to a lesser extent in advanced combustion modes with $0.45 < \Phi' < 0.65$, e.g. with SACI, will likely require higher unburned gas temperatures than was simulated in these calculations. Although not shown in the figure, at the NOx limits, the maximum temperature is less than ~ 2100 K and maximum pressure is less than ~ 150 bar. Maximum motoring pressure, P_{TDC} , i.e. compression pressure in

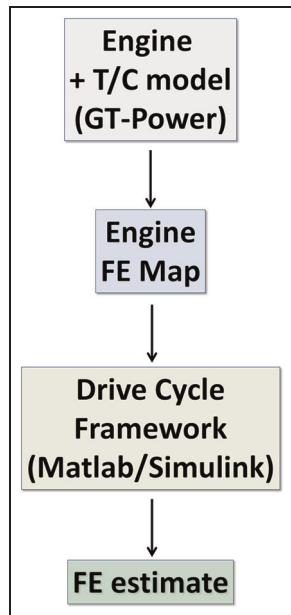


Figure 22. Schematic of procedure for estimating vehicle fuel economy (FE).

the absence of combustion, is less than ~ 80 bar. Up to ~ 20 bar BMEP and inlet pressure of 3.0 bar, the 50% efficiency turbocharger can supply just enough boost to avoid a pumping penalty; above this point, the turbocharger provides additional work at the expense of higher Φ' , temperature and NOx, but does not achieve better efficiency because of the accompanying change in thermodynamic properties.

Vehicle fuel economy

To understand the benefits of advanced combustion technologies in terms of drive-cycle fuel economy, the comprehensive engine to drive-cycle modeling framework presented by Ortiz-Soto et al.⁴⁷ was employed. Figure 22 shows a schematic of the processes involved. First, the GT-Power model, together with the ideal turbocharger relationships outlined above, was exercised over a suitable range of speeds and loads to generate fuel economy maps depending on the particular operating strategy chosen. Then, the maps were input to the framework with suitable drive train parameters to generate the fuel economy estimates.

Engine maps

The six engine strategies considered are shown in Figure 23 where brake efficiency is plotted versus BMEP at 2400 r/min for a number of combinations of combustion mode, air handling, and engine sizing, each indicated by a heavy numbered line. The first three strategies (1–3) cover the load range up to BMEP of ~ 10 bar and are intended to represent a base engine size; the last three strategies (4–6) cover the expanded load range up to BMEP ~ 25 bar and would be implemented in downsized engines with equivalent performance. The

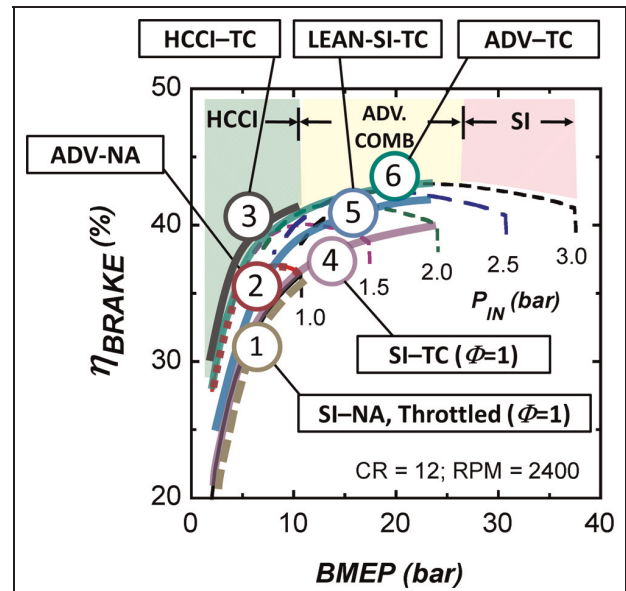


Figure 23. Six engine strategies used to generate fuel economy maps used for vehicle fuel economy projections. Turbocharger efficiency 50%. Brake efficiency versus load for 2400 r/min.

figure clearly shows a benefit due to increasing load and downsizing. As noted earlier, this is due to the diminished influence of frictional losses at high loads and occurs regardless of the combustion mode. All the engines were modeled with identical geometry, fixed valve timing and a compression ratio of 12:1, as specified in Table 1. Thus, the engine modes vary only in operating conditions. Turbocharger efficiency is set at 50% for all boosted cases.

Strategy 1 (SI-NA) represents current stoichiometric, SI, throttled engines; strategy 2 (ADV-NA) is a naturally aspirated unthrottled engine including HCCI and advanced combustion as well as SI at the highest loads; strategy 3 (HCCI-TC) is a boosted engine with only HCCI combustion. Since its load does not go above ~ 10 bar, this engine is not downsized. Strategy 4 (SI-TC) is a stoichiometric, SI, turbocharged engine. Because it operates with stoichiometric mixtures, it requires a boost of only 2 bar to achieve BMEP of 25 bar. Strategy 5 (Lean-SI-TC) is a lean ($\Phi = 0.75$), SI, turbocharged engine requiring a somewhat higher boost level of 2.5 bar to achieve the same maximum load. This strategy is similar to the HEDGE concept,³ but is diluted with air rather than EGR for compatibility with the other strategies considered. As such, it represents a potential optimal application of SI technology. Finally, strategy 6 (ADV-TC) corresponds to the optimal air dilute case shown in Figure 21. It employs both HCCI and advanced combustion, achieves loads up to BMEP ~ 25 bar with boost to 3 bar, and retains low-temperature combustion throughout its operating range.

Engine maps were generated for each of the six strategies by varying the parameters over the ranges shown in Table 4. Although calculations were carried out up to 3 bar intake pressure, the maps only include conditions resulting in loads less than 25 bar BMEP in order

Table 4. Parameter ranges for maps.

Case	Combustion mode	Air handling	Intake pressure (bar)	Equivalence ratio Φ	Engine speed (r/min)
1	Stoich-SI	NA	0.2–1.0	1.0	500–6000
2	Advanced	NA	1.0	0.2–1.0	500–6000
3	HCCI	TC	1.0–3.0	0.2–0.45	500–6000
4	Stoich-SI	TC	0.2–3.0	1.0	500–6000
5	Lean-SI	TC	0.2–3.0	0.75	500–6000
6	Advanced	TC	1.0–3.0	0.2–1.0	500–6000

to realistically represent practically achievable loads in current boosted engine hardware. For the ADV-TC engine as described earlier, the most efficient combination of equivalence ratio and boost for each operating point is selected to generate the map. Maximum intake pressure included on the maps was ~ 2 bar for the SI-TC engine, ~ 2.5 bar for the lean-SI-TC engine, and 3 bar for the HCCI-TC and ADV-TC engines. The engine mapping results are presented in Figure 24. The stoichiometric SI-NA engine map shows the typical upper envelope found in conventional gasoline SI engines and qualitatively agrees with engine maps available in the literature.³⁸ Because no high-load enrichment was used in the model, there is no ‘fuel island’. Peak load and minimum fuel consumption values are reasonable; however, the assumed combustion efficiency of 100% slightly reduces the minimum BSFC compared to published results. The ADV-NA engine shows the same maximum load curve, but lean operation significantly improves fuel consumption, where the 230 g/kW-hr contour now covers a much wider region of the map. In the very low load regions (BMEP $< \sim 1$ bar) of both the HCCI and advanced combustion maps, it was assumed that throttled, stoichiometric conditions would be used because of combustion stability and misfire under the highly dilute conditions.

Engine sizing

To simplify calculations, all engines are represented by the maps shown above developed for the 90 mm bore engine geometry given in Table 1. In order to take full advantage of boosted strategies, it is necessary to match displacement to the increased mean effective pressures, either by reduced number of cylinders or by using smaller bores. Downsizing by reducing the number of cylinders will not affect the validity of the map results. The potential effect of bore size reduction was evaluated based on a small set of simulations with bore sizes ranging from the base of 90 mm to 72 mm. The change in brake efficiency was influenced by the trade-off between friction and heat-transfer losses depending on whether engine speed was held constant (brake efficiency gain of 0.2%) or increased to maintain constant piston speed (loss of 0.2%). In view of these small effects, the engine displacement can be varied over a

wide range of displacements (1–4 l) without significant error due to use of the single-engine map.

Vehicle and drive train

A full vehicle model was developed in MATLAB/Simulink⁴⁸ for a front-wheel drive configuration with a manual transmission. A mid-size sedan was the chosen vehicle platform, and a summary of the important parameters is provided in Table 5. Each engine strategy was matched to a particular engine size and configuration, given the geometry of the single-cylinder engine model, and realistic progression of engine technologies and design. The baseline engine was taken to be a naturally aspirated SI, six-cylinder, 3.3 l engine. To maintain torque and performance, the advanced combustion naturally aspirated and the boosted HCCI engines were of the same engine size. Peak torque and power were 281 N.m and 162 kW, respectively. The boosted SI and advanced combustion engines were both downsized to a four-cylinder, 1.4 l configuration. This reduction in displaced volume compensated for the increased specific load so that peak torque and power remained the same as the naturally aspirated engines. The city (UDDS) and highway (HWFET) EPA Dynamometer Driving Cycles⁴⁹ were employed for drive-cycle fuel economy evaluation.

Clutch friction was modeled using a hyperbolic tangent function.⁵⁰ For the purpose of control simplicity, the transmitted clutch torque was calculated algebraically as a fraction of requested engine torque based on current engine and transmission input speed (clutch slip). A robust forward-looking driver model was employed for engine load and braking control.⁵¹ To clearly understand fuel economy trends as a result of engine configuration, the transmission shifting strategy was developed based on absolute torque, instead of accelerator position or engine load percent. The shifting schedule was initially developed for the baseline SI-NA, six-cylinder, 3.3 l engine, and then fixed for all simulations, with provisions taken to ensure adequate behavior over the torque ranges available from the various engines.

The city, highway, and combined vehicle fuel economy results are shown in Table 6 for the six strategies, labeled in the same way as in the mapping figures; combined results are also plotted in Figure 25. The absolute

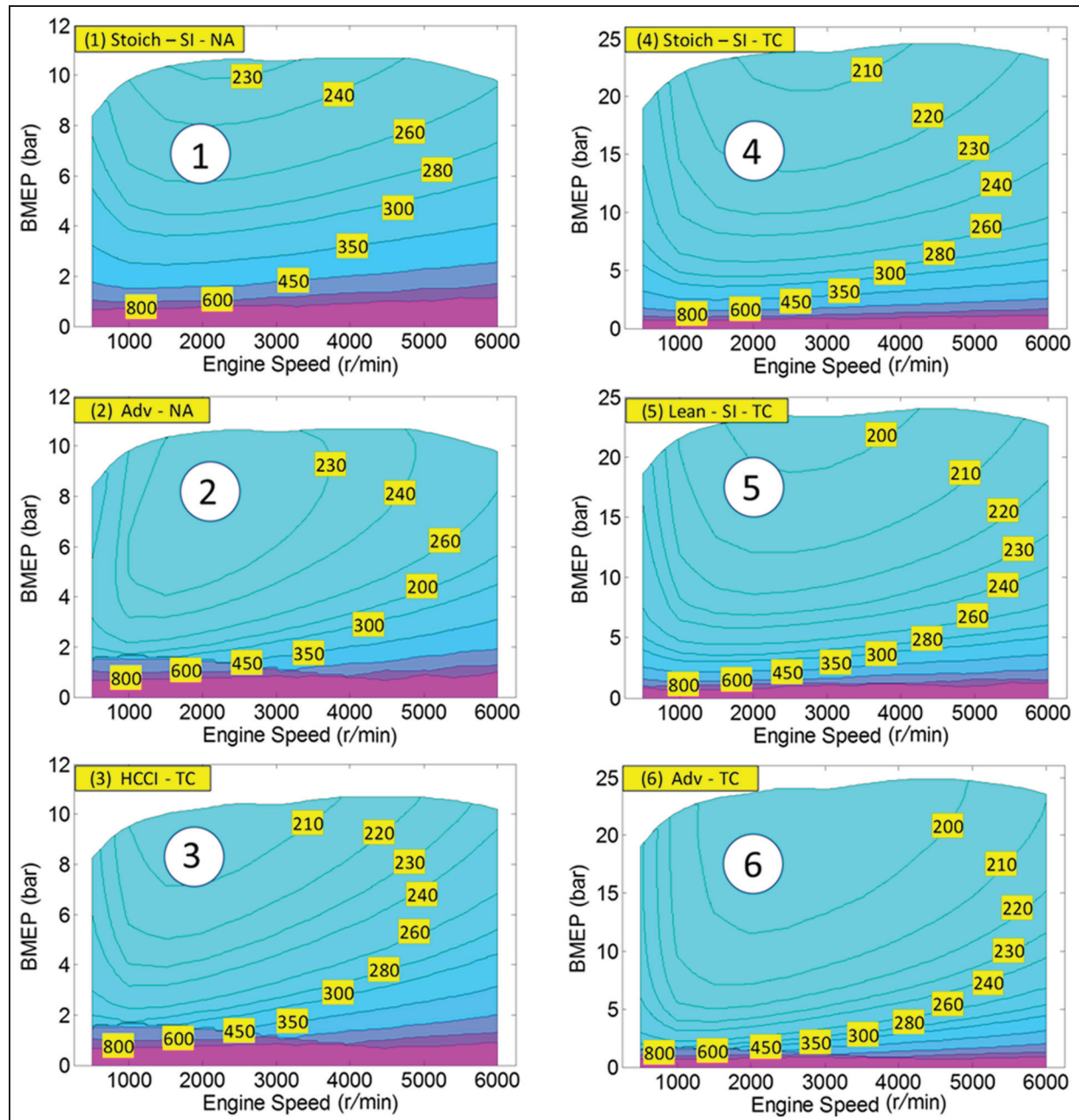


Figure 24. Engine BSFC maps for the six strategies. Contour labels give BSFC values in g/kWh.

Table 5. Drive train parameters.

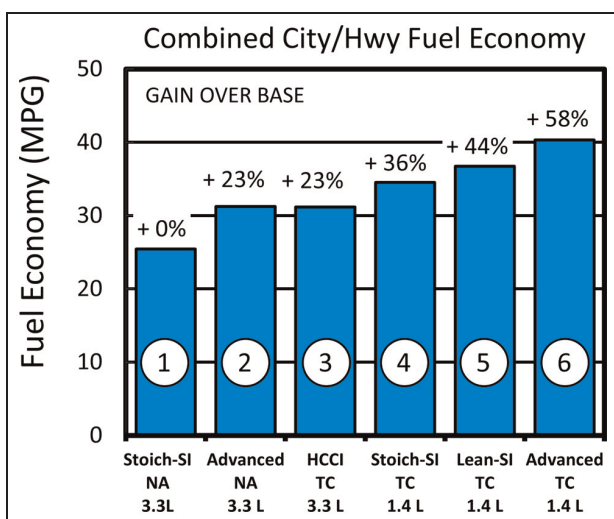
Driveline configuration	Front-wheel drive			
Vehicle weight	1490 kg			
Frontal area	2.94 cm ²			
Drag coefficient	0.33			
Wheels/tires	205/60 R16			
Transmission	Six-speed with friction clutch			
Transmission gear ratios	1 st 2 nd 3 rd	3.45 1.84 1.31	4 th 5 th 6 th	1.03 0.84 0.68
Final drive	4.58			

values are realistic but somewhat optimistic compared with published EPA values for the SI-NA strategy and this vehicle size. This may be because combustion efficiency was assumed to be 100%; also, fuel economy numbers are unadjusted, i.e. no downward corrections were made for consumer use factors such as cold start, as is done to obtain EPA sticker fuel economy.

Figure 25 shows that significant gains can be achieved either by introducing advanced combustion or by boosting and downsizing. Maximum gain is achieved by combining advanced combustion and downsizing. Strategies 2 and 3 incorporate advanced combustion or boosted HCCI combustion, but keep engine size

Table 6. Vehicle fuel economy results.

Case	Combustion mode	Air handling	Size	City (mpg)	Hwy (mpg)	Combined (mpg)
1	Stoich-SI	NA	3.3 l	23.3	28.7	25.4
2	Advanced	NA	3.3 l	27.8	36.9	31.3
3	HCCI	TC	3.3 l	27.7	36.8	31.2
4	Stoich-SI	TC	1.4 l	31.4	39.3	34.5
5	Lean-SI	TC	1.4 l	33.2	42.2	36.7
6	Advanced	TC	1.4 l	36.4	46.5	40.3

**Figure 25.** Projected combined City/Hwy fuel economy for the six engine strategies. Labels indicate percent gain over the base SI engine.

constant in order to maintain similar performance. The gain over the base engine for these strategies is $\sim 23\%$ and is due primarily to thermodynamic gains affecting gross efficiency. Downsizing the engine and boosting provides additional gains to brake efficiency for strategies 4, 5, and 6 due to the increased engine loading and reduced relative friction. Within the downsized group, the stoichiometric and lean SI show gains of 36% and 44%, respectively, while the advanced combustion provides the maximum 58% gain.

Despite the significant amount of boost and downsizing, most of the time the engines operated at less than half their maximum torque and rarely entered the optimum fuel economy regions. This is a result of the fact that equal performance was maintained for all engine modes. Further gains could be achieved with some performance penalty, or if hybridization was used for additional load management.

Discussion

The analysis described here makes use of many simplifying assumptions such as constant burn rate and 100% combustion efficiency. The accuracy could be improved by improved combustion, heat-transfer, and friction models, and more realistic turbocharger

characteristics. Nevertheless, the model contains all the key thermodynamic processes involved in determining engine efficiency, and the general features shown in the results are expected to be qualitatively valid. In practice, however, achieving the optimum fuel economy identified by the thermodynamics is subject to a number of constraints. Most important is the need to have reliable, knock-free combustion at the conditions in the analysis. Other constraints are introduced by the air and EGR handling system, which will influence the range of possible intake temperatures. These constraints may have a negative effect on turbocharger efficiency because of enthalpy changes. Engine efficiency can also be affected due to increased heat transfer and reduced γ caused by increased charge temperatures often required for advanced combustion modes and resulting from the use of large amounts of EGR. Combustion mode may adversely affect emissions such as NOx and particulates, imposing further constraints on practical combustion regimes. In addition, a boosted advanced combustion engine is likely to have increased friction due to more robust bearings. As a result of these constraints, the potential gains relative to current SI engines represent an upper limit.

In spite of the model limitations, the results show that the thermodynamic benefit of using advanced combustion modes is largely independent of the additional frictional gains provided by increasing engine load levels. The best vehicle fuel economy projections are for the boosted/downsized advanced combustion engine, with the boosted/downsized, lean/dilute SI strategy providing almost as much gain. The results suggest that future engines should be equipped with turbochargers, regardless of the combustion mode. Also, gains from hybridization appear possible for any of the configurations studied because none of the simulations showed much time spent at maximum load.

For gasoline SI engines, significant efficiency gains are possible, with the potential to reach diesel-like fuel economy. It is worth noting that diesel engines for the most part operate in the same thermodynamic region as the advanced combustion modes identified here, although the combustion mode and control mechanisms are different with possible effects on efficiency. For example, radiation is a significant source of heat loss in diesels and not in SI engines. On the other hand, diesel engines do not, as a rule, have losses due to crevice hydrocarbons. The challenges for gasoline engines

are well known, especially for automotive applications. Achieving reliable knock-free combustion under high dilution conditions while avoiding high emissions, all in the transient environment of a modern turbocharger system will not be easy. However, rapid advances are being made in both turbomachinery and engine control systems such as variable geometry turbochargers and variable valve actuation, which will play a key role in enabling advanced combustion and avoiding knock in SI systems.

Summary and conclusions

Summary

A parametric study has been carried out to evaluate the fuel economy potential of advanced combustion (ultra-lean or EGR dilute) in the context of an automotive gasoline fueled turbocharged engine. The simulation was carried out with GT-Power and employed ideal turbochargers with constant efficiencies. The engine had a compression ratio of 12, bore/stroke of 90/100 mm, and had conventional valve timing. A constant combustion burn duration of 25 CA degrees was assumed with CA50 phasing of 10° ATC. Standard Woschni heat transfer was used along with the Chen–Flynn friction correlation. Both air and EGR dilution were varied to obtain a range of ‘fueltocharge’ equivalence ratios $\Phi' \equiv \Phi(1 - \text{EGR})$ from 0.2 to 1.0. Inlet pressure was varied from 1 to 3 bar, and speed ranged from 500 to 6000 r/min. Turbocharger efficiencies of 40%, 50%, and 60% were considered. Engine maps were constructed for a number of combustion and boosting strategies, and the strategies evaluated in a vehicle drive-cycle framework to estimate the potential overall fuel economy gains.

Conclusions

Based on an extensive parametric study with the GT-Power engine and a vehicle framework model, the following conclusions can be made.

1. Dilution with either air or EGR provides a benefit to gross efficiency due to improved thermodynamic properties, partly because of composition changes and partly because of reduced temperatures. EGR dilution provides almost as much improvement as air dilution.
2. Raising the load generally improves brake efficiency because of reduced relative friction losses.
3. Turbocharging helps net efficiency by permitting higher load operation and by providing positive work (negative PMEP) under some conditions.
4. For a given turbocharger efficiency, best brake efficiency is obtained by simultaneously increasing boost and the ‘fuel-to-charge’ equivalence ratio Φ' as brake load is increased, thus optimizing the tradeoffs between friction losses, gas property effects, and turbocharger effectiveness.

5. Higher turbocharger efficiency allows higher dilution at a given brake load and extends the load range for a given combustion mode: HCCI (maximum Φ' of ~ 0.45) can be used up to BMEP of ~ 14 bar with a 60% efficient turbocharger, but only ~ 5 bar with a 40% efficient turbocharger.
6. For a 50% efficient turbocharger, peak brake engine efficiency at 2400 r/min is $\sim 41\%$ with HCCI (Φ' of 0.45) at ~ 11 bar BMEP; and $\sim 43\%$ with advanced combustion (Φ' of 0.6) at ~ 25 bar BMEP. With the same modeling assumptions, the maximum efficiency for a current, stoichiometric, throttled naturally aspirated engine is estimated to be $\sim 36\%$.
7. For a 50% efficient turbocharger and engine at 2400 r/min, the NOx limit of 0.26 g/kWh can be achieved with advanced combustion up to 18 bar BMEP with air dilution and 25 bar BMEP with stoichiometric EGR.
8. Model-generated engine maps for various combinations of combustion mode, boosting, and sizing strategies were assessed with a vehicle drive-cycle model with 50% turbocharger efficiency. The results showed that significant vehicle fuel economy gains could be achieved relative to the baseline, throttled stoichiometric engine:
 - (a) a gain of $\sim 23\%$ in combined city/highway fuel economy was seen for either naturally aspirated advanced or boosted HCCI combustion in a current sized engine;
 - (b) gains of 36%, 44%, and 58% in combined city/highway fuel economy were projected for stoichiometric SI, lean/dilute SI, and advanced combustion, respectively, in boosted, down-sized engines.
9. The benefits of combustion mode and boosting/downsizing appear to be relatively independent, with the best results obtained by combining both features. Hybridization is likely to provide additional gains.

Funding

This work was supported by the US Department of Energy under contract DE-EE0000203, ‘A University Consortium on Efficient and Clean High Pressure Lean Burn (HPLB) Engines’.

Acknowledgements

The authors gratefully acknowledge the help of graduate students Sotirios Mamalis and Laura Olesky for providing modeling assistance and validation data, and Dr Stani Bohac for many valuable discussions.

References

1. Caton JA. An assessment of the thermodynamics associated with high-efficiency engines. In: *ASME 2010 ICE*

- Fall Technical Conference*, San Antonio, TX. ASME, 2010.
2. Kalghatgi G. Auto-ignition quality of practical fuels and implications for fuel requirements of future SI and HCCI engines. SAE paper 2005-01-0239, 2005.
 3. Pirault J-P, Ryan TW, Alger TF, et al. Performance predictions for high efficiency stoichiometric spark-ignited engines. SAE paper 2005-01-0995, 2005.
 4. Dec JE and Sjoberg M. A parametric study of HCCI combustion – the sources of emissions at low loads and the effects of GDI fuel injection. SAE paper 2003-01-0752, 2003.
 5. Christensen M, Johansson B, Amneus P, et al. Supercharged homogeneous charge compression ignition. SAE paper 980787, 1998.
 6. Persson H, Agrell M, Olsson J-O, et al. The effect of intake temperature on HCCI operation using negative valve overlap. SAE paper 2004-01-0944, 2004.
 7. Advanced Reciprocating Engine Systems (ARES), US Department of Energy EERE, Industrial Technologies Program, <http://www1.eere.energy.gov/industry/distributedenergy/m/ares.html> (2010).
 8. Alger T. SwRI's HEDGE – SwRI's concept for high efficiency dilute gasoline engines for automotive medium duty and off-road applications. SAE High Efficiency IC Engines – Panel Discussion. SAE paper, 2009.
 9. Alger T, Gingrich J, Mangold B, et al. A continuous discharge ignition system for EGR limit extension in SI engines. SAE paper 2011-01-0661, 2011.
 10. DeFilippo A, Saxena S, Rapp V, et al. Extending the lean stability limits of gasoline using a microwave-assisted spark plug. SAE paper 2011-01-0663, 2011.
 11. Scussel AJ, Simko AO and Wade WR. The Ford PROCO engine update. SAE paper 780699, 1978.
 12. Noma K, Iwamoto Y, Murakami N, et al. Optimized gasoline direct-injection engine for the European market. SAE paper 980150, 1998.
 13. Sjöberg M, Dec JE and Cernansky NP. Potential of thermal stratification and combustion retard for reducing pressure-rise rates in HCCI engines based on multi-zone modelling and experiments. SAE paper 2005-01-0113, 2005.
 14. Snyder J, Droniou N, Dec, et al. PLIF measurements of thermal stratification in an HCCI engine under fired operation. SAE paper 2011-01-1291, 2011.
 15. Manente V, Johansson B and Tunestal P. Partially premixed combustion at high load using gasoline and ethanol, a comparison with diesel. SAE paper 2009-01-0944, 2009.
 16. Yang Y, Dec J, Droniou N, et al. Partial fuel stratification to control HCCI heat release rates: fuel composition and other factors affecting pre-ignition reactions of two-stage ignition fuels. SAE paper 2011-01-1359, 2011.
 17. Hanson RM, Kokjohn SL, Splitter DA, et al. An experimental investigation of fuel reactivity controlled PCCI combustion in a heavy-duty engine. SAE paper 2010-01-0864, 2010.
 18. Manofsky L, Vavra J, Babajimopoulos A, et al. Bridging the gap between HCCI and SI: spark-assisted compression ignition. SAE paper 2011-01-1179, 2011.
 19. Persson H, Johansson B and Remon A. The effect of swirl on spark-assisted compression ignition (SACI). SAE paper 2007-01-1856, 2007.
 20. Szybist J, Nafziger E and Weall A. Load expansion of stoichiometric HCCI using spark assist and hydraulic valve actuation. SAE paper 2010-01-2172, 2010.
 21. Yun H, Wermuth N and Najt P. Extending the high load operating limit of a naturally-aspirated gasoline HCCI combustion engine. SAE paper 2010-01-0847, 2010.
 22. Chadwell C, Alger T, Roberts C, et al. Boosting simulation of high efficiency alternative combustion mode engines. SAE paper 2011-01-0358, 2011.
 23. Caton JA. The destruction of exergy during the combustion process for a spark-ignition engine. In: *ASME ICE Fall Technical Conference*, San Antonio, TX. ASME, 2010.
 24. Farrell JT, Stevens JG and Weissman WA. Second law analysis of high efficiency low emission gasoline engine concepts. SAE paper 2006-01-0491, 2006.
 25. Teh KY, Miller SL and Edwards CF. Thermodynamic requirements for maximum internal combustion engine cycle efficiency. Part 1: optimal combustion strategy. *Int J Engine Res* 2008; 9: 449–465.
 26. Teh KY, Miller SL and Edwards CF. Thermodynamic requirements for maximum internal combustion engine cycle efficiency. Part 2: work extraction and reactant preparation strategies. *Int J Engine Res* 2008; 9: 467–481.
 27. GT-Suite V7.2, Gamma Technologies Inc, <http://www.gtisoft.com>.
 28. Morel T, Rackmil CI, Keribar R, et al. Model for heat transfer and combustion in spark ignited engines and its comparison with experiments. SAE paper 880198, 1988.
 29. Watson N and Janota MS. *Turbocharging the internal combustion engine*. John Wiley and Sons, 1982.
 30. Woschni G. Equation for the instantaneous heat transfer coefficient in the internal combustion engine. SAE paper 670931, 1967.
 31. Heywood JB. *Internal combustion engine fundamentals*. New York: McGraw-Hill, 1988.
 32. Chen SK and Flynn PF. Development of a single cylinder compression ignition research engine. SAE paper 650733, 1965.
 33. Bishop IN. Effect of design variables on friction and economy. SAE paper 812A. *SAE Trans* 1964; 73: 334–358 (640807).
 34. Patton KJ, Nitschke RG and Heywood JB. Development and evaluation of a friction model for spark-ignition engines. SAE paper 890836, 1989.
 35. Thring RH. Engine friction modeling. SAE paper 920482, 1992.
 36. Kouremenos DA, Rakopoulos CD and Hountalas DT. Development of a detailed friction model to predict mechanical losses at elevated maximum combustion pressures. SAE paper 2001-01-0333, 2001.
 37. Sandoval D and Heywood JB. An improved friction model for spark-ignition engines. SAE paper 2003-01-0725, 2003.
 38. Tsuchiya T, Hosoi H, Hoshi K, et al. Newly developed inline 4 AR series SI engine. SAE paper 2009-01-1048, 2009.
 39. Cho K-W, Assanis D, Filipi Z, et al. Experimental investigation of combustion and heat transfer in a direct-injection spark ignition engine via instantaneous combustion chamber surface temperature measurements. *Proc IMechE, Part D: J Automobile Engineering* 2008; 222: 2219–33.

40. Caton JA. Comparisons of global heat transfer correlations for conventional and high efficiency reciprocating engines. In: *ASME Internal Combustion Engine Division 2011 Fall Technical Conference*, Morgantown, WV October 2011. ASME, 2011.
41. Hohenberg GF. Advanced approaches for heat transfer analysis. SAE paper 790825, 1979.
42. Chang J, Güralp O, Filipi Z, et al. New heat transfer correlation for an HCCI engine derived from measurements of instantaneous surface heat flux. SAE paper 2004-01-2996, 2004.
43. Kawamoto N, Naiki K, Kawai T, et al. Development of new 1.8-liter engine for hybrid vehicles. SAE paper 2009-01-1061, 2009.
44. Caris DF and Nelson EE. A new look at high compression engines. SAE paper 590015. *SAE Trans* 1959; 67: 112–122.
45. Dec JE and Yang Y. Boosted HCCI for high power without engine knock and with ultra-low NOx emissions – using conventional gasoline. SAE paper 2010-01-1086, 2010.
46. Yang Y, Dec J, Droniou N, et al. Boosted HCCI combustion using low-octane gasoline with fully premixed and partially stratified charges. SAE paper 2012-01-1120, 2012.
47. Ortiz-Soto E, Assanis D and Babajimopoulos A. A comprehensive engine to drive-cycle modeling framework for the fuel economy assessment of advanced engine and combustion technologies. *Int J Engine Res* 2011; 12: 1–19.
48. MATLAB Version 7.80.347 (R2009a). Natick, MA: The MathWorks Inc, 2009.
49. Dynamometer Driving Cycles US. Environmental Protection Agency, <http://www.epa.gov/nvfel/testing/dynamo-meter.htm> (2010).
50. Andersson S, Soderberg A and Bjorklund S. Friction models for sliding dry, boundary and mixed lubricated contacts. *Tribol Int* 2007; 40: 580–587.
51. Lin C-C, Filipi Z, Wang Y, et al. Integrated feed-forward hybrid electric vehicle simulation in SIMULINK and its use for power management studies. SAE paper 2001-01-1334, 2001.

Appendix I

Notation

C_P, C_V	specific heats at constant pressure and volume	$\gamma, \gamma_C, \gamma_T$	ratio of specific heats C_P/C_V ; subscripts for compressor and turbine
f_{EGR}	fraction of exhaust gas recycled externally into intake stream	Φ	fuel air equivalence ratio (F/A)/(F/A) _{ST}
f_{RES}	fraction of residual gas (previous cycle contents in cylinder not considering external exhaust gas recirculation)	Φ'	fuel-to-charge equivalence ratio (F/Charge)/(F/A) _{ST}
\dot{m}_C, \dot{m}_T	mass flow through the compressor and turbine	η_{BRAKE}	brake engine efficiency
$P_{\text{IN}}, P_{\text{EX}}, P_{\text{ATM}}$	intake, exhaust and atmospheric pressures (bar)	η_C	compressor efficiency
P_{MAX}	maximum cylinder pressure (bar)	η_{GROSS}	gross engine efficiency (over 360°)
$T_{\text{IN}}, T_{\text{EX}}, T_{\text{ATM}}$	intake, exhaust and atmospheric temperatures (K)	η_{MECH}	turbocharger mechanical efficiency
T_{MAX}	maximum cylinder temperature (K)	η_{NET}	net engine efficiency (over 720°)
U_P	mean piston speed (m/s)	η_{OTC}	overall turbocharger efficiency
		η_T	turbine efficiency
Abbreviations			
ADV			advanced combustion
ATC			After Top Center
BMEP			brake mean effective pressure (bar)
BSFC			brake specific fuel consumption (g/kWh)
BSNOx			Brake Specific Nitrogen Oxides (g/kWh)
CA			Crank Angle
CR			Compression Ratio
CA50			crank angle at 50% mass fraction burned
EGR			exhaust gas recirculation (mass fraction)
EIVC			early intake valve closing
EVO			Exhaust Valve Open
EVC			Exhaust Valve Close
$F/A, (F/A)_{\text{ST}}$			fuel air ratio, stoichiometric fuel air ratio
FMEP			friction mean effective pressure (bar)
GMEP			gross mean effective pressure (bar)
HCCI			homogeneous charge compression ignition
HD			heavy duty
HEDGE			high-efficiency dilute gasoline engine
IVO			Intake Valve Open
IVC			Intake Valve Close
LD			light duty
NMEP			net mean effective pressure (bar)
PMEP			pumping mean effective pressure (bar)
RGF			total residual gas fraction
SACI			referring to all burned gas in the cylinder
SI			spark assisted compression ignition
T/C			spark ignition
TDC			turbocharger
			top dead center